Colloidal Synthesis of Hollow Cobalt Sulfide Nanocrystals

Yadong Yin,[1,2 †] Can K. Erdonmez,[2 †] Andreu Cabot,[2] Steven Hughes,[3] A. Paul. Alivisatos[1,2,3*]

[1]The Molecular Foundry and [2]Materials Science Division at the Lawrence Berkeley National Laboratory, [3]Department of Chemistry, University of California at Berkeley, Berkeley, CA 94720, USA.

[†] These authors contributed equally to this work.

[*] Correspondence should be addressed to A.P.A. (alivis@berkeley.edu).

Abstract

Formation of cobalt sulfide hollow nanocrystals through a mechanism similar to the Kirkendall Effect has been investigated in detail. It was found that performing the reaction at >120˚C leads to fast formation of a single void inside each shell, whereas at room temperature multiple voids are formed within each shell, which can be attributed to strongly temperature-dependent diffusivities for vacancies. The void formation process is dominated by outward diffusion of cobalt cations; still, significant inward transport of sulfur anions can be inferred to occur as the final voids are smaller in diameter than the original cobalt nanocrystals. Comparison of volume distributions for initial and final nanostructures indicates excess apparent volume in shells implying significant porosity and/or a defective structure. Indirect evidence for shells to fracture during growth at lower temperatures was observed in shell size statistics and TEM of as-grown shells. An

idealized model of the diffusional process imposes two minimal requirements on material parameters for shell growth to be obtainable within a specific synthetic system.

Keywords: Hollow Nanocrystals, Kirkendall Effect, Synthesis, Colloidal Nanocrystals, Diffusion

1. Introduction

We recently demonstrated that by introducing an oxidizing, molecular species into a colloidal solution of metallic nanocrystals at moderate temperature, hollow particles, each one with a single well-defined void can be formed.[1] Other workers had occasionally observed void formation during chemical modification or synthesis of nanostructures, either attributing these observations to materials-specific processes [2-4] or noting morphology of the product without comment on mechanism.[5, 6] Bulk studies had established for some of the compositions that we studied that the reaction between the metal and the molecular species is facilitated predominantly by diffusive transport of the metallic species through the growing shell. Thus, we attributed formation of hollow nanocrystals to the impermeability of the shell material to the dissolved oxidizing species. Void formation upon oxidation of metals is a common phenomenon conceptually related to the Kirkendall Effect known to result in porosity or deformations due to differing diffusivities of the different components in a diffusion couple.

The demonstration by Smigelskas and Kirkendall of net material flux across an interface between two different metal specimens upon annealing was a key experiment in the development of solid state physics and materials science,[7, 8] establishing vacancy-

assisted hopping as the main mode of atomic transport. In the simplest picture of this process, a vacancy flow balancing the net material flow results, with vacancies accumulating and condensing into voids on the side of the faster-diffusing species. In bulk specimens, the total volume of voids formed typically turns out to be orders of magnitude smaller than the net volume of material transported across the interface position. Much of the material flow instead results in deformation, sometimes on a visible scale, of the diffusion couple. The deformation is driven by stress fields due to the increased vacancy concentration; as the deformation proceeds, a large fraction of vacancies are consumed by moving dislocations before they can nucleate voids. Porosity may become more pronounced in specimens with higher surface-to-volume ratio and greater crystalline perfection due to confinement of vacancies into smaller volumes and an enhancement of vacancy injection rate.[9] Thus, formation of a single void in each colloidal nanocrystal sample is naturally understood as a case of Kirkendall porosity where each crystal is sufficiently small that it can support only one void. Based on this explanation, the methodology should generalize readily to production of hollow nanostructures composed of diverse compounds and alloys. Indeed, the concept of the Kirkendall Effect has recently been applied to successfully synthesize various hollow oxide nanostructures, illustrating its potential in generating novel nanostructured materials.[10-12] Furthermore, given the generality of the explanation, we suggest that the Kirkendall Effect plays a role in some of the earlier observations of toroid morphologies[13-16] and hollow nanostructures.[2-6]

The morphology of our hollow nanostructures and the diffusional process underlying their formation are much simpler in comparison to analogous bulk systems,

inviting ‘mechanistic’ studies that characterize the evolution of hollow nanostructures formed from solid starting nanoparticles. Ideally, such studies would characterize both the chemical and the morphological features of the nanoparticles being transformed. Diffusional kinetics have already been observed using in situ IR spectroscopy to track the oxidation of solid Fe_3O_4 nanoparticles into solid Fe_2O_3 particles.[17] This study was facilitated by a NIR peak strongly characteristic of the starting material and a simple chemistry where the solvent is also the oxidizing agent. We have not yet formulated a synthetic system where chemical transformation can be monitored so unambiguously; instead, here we focus on morphological evolution and its dependence on reaction conditions. In particular, we study the formation of hollow cobalt sulfide structures upon sulfidation of cobalt nanospheres. Electron microscopy and x-ray diffraction are used as the main tools to characterize the dependence of particle shape, crystallographic phases present and size distribution of particles on the synthesis temperature and synthesis time. Trends connecting final product morphology to the reaction conditions and starting particle diameter are also reported. The results support the picture of a vacancy-assisted diffusional process. The data also contains evidence for additional processes accompanying shell growth which modify product morphology from one expected from a simple diffusion-based picture. Our discussion of the origin of these deviations, as well as the highly idealized mathematical model of the diffusional process that follows, highlight phenomena that are likely to be generally involved in the production of hollow nanostructures based on the Kirkendall Effect. A better understanding of the mode of growth should assist future efforts to extend synthetic control over geometrical, thermodynamic or crystallographic properties of similarly prepared hollow

nanostructures, which may find uses in fields as diverse as catalysis, ultrasound imaging, low-dielectric materials and drug delivery. Considering that until now, the main technological motivation for studying Kirkendall porosity has been its negative effect on adhesion or mechanical reliability at interfaces, it is fitting that a cornerstone of materials science may finally find a 'constructive' application in the synthesis of novel structures on the nanometer scale.

2. Results

As we reported earlier, reaction of colloidal Co nanoparticles with molecular sulfur in solution produces hollow nanoparticles. Performing the sulfidation reaction at ~180˚C results in sulfide shells composed of either the linnaeite (Co_3S_4) or the cobalt pentlandite (Co_9S_8) phase, depending precisely on the sulfur-to-cobalt molar ratio used in the synthesis. When the sulfur-to-cobalt molar ratio is less than 8:9, Co_9S_8 is the only sulfide phase observed in XRD patterns of the product. While CoS_2 is also a stable phase at the reaction temperature, only Co_3S_4 was detected up to molar sulfur-to-cobalt ratios of 8:1, possibly due to a kinetic barrier to the formation of CoS_2 at the synthesis temperature. Research on sulfidation of bulk Co at significantly higher temperatures indicates that the formation of CoS_2 is preceded by a long nucleation period.[18]

The time required to form hollow particles decreases dramatically with the increase of temperature as expected for a thermally activated process. Furthermore, the morphological evolution of particles changes significantly with temperature in a way that demonstrates the diffusional processes at play. Figure 1 shows TEM images of initial cobalt nanocrystals and their sulfides after reaction at room temperature (Fig. 1A), 120°C

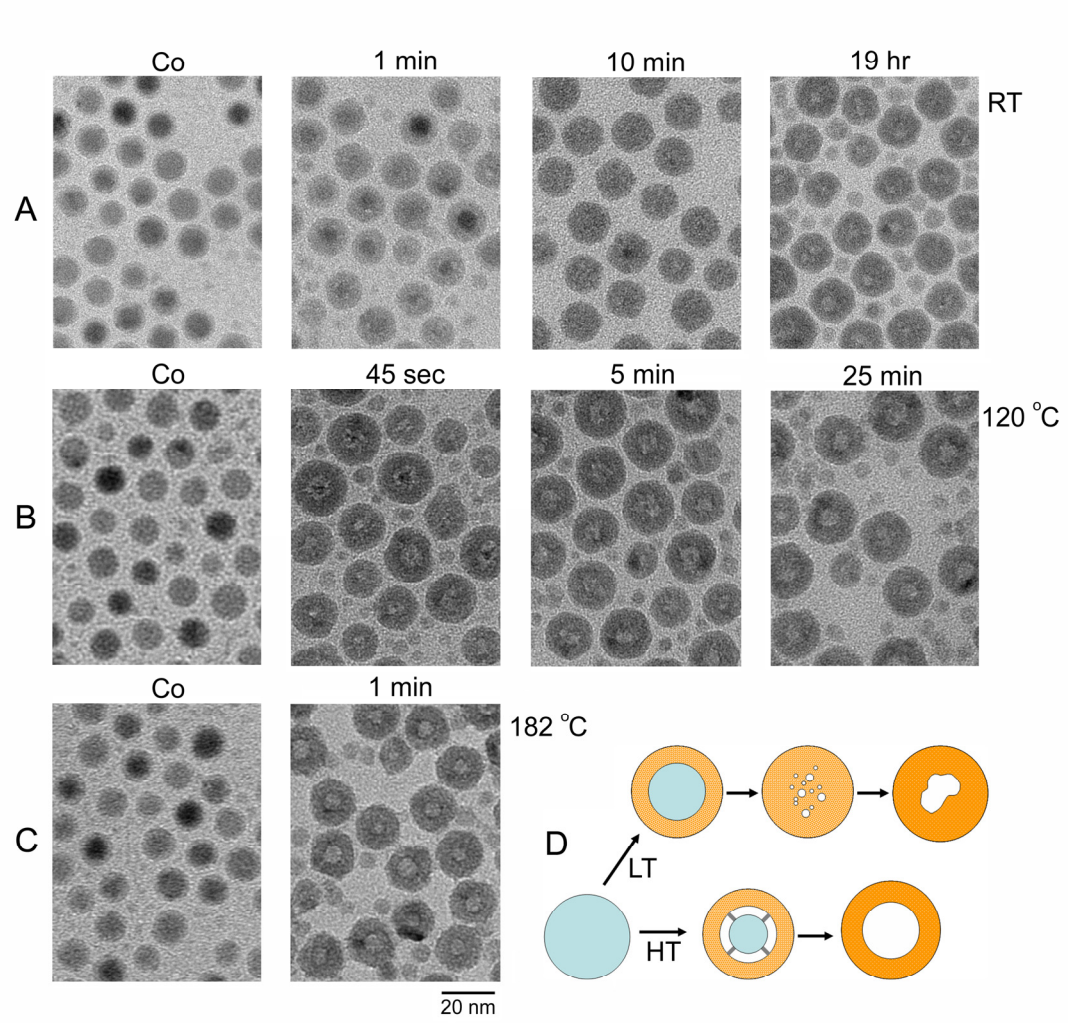

Figure 1. TEM images of nanoparticle morphology during sulfidation of Co nanocrystals using a Co/S molar ratio equal to ¾ (A) at room temperature; images show, from left to right, original cobalt particles, particles at 1 min, 10 min, and 19 hours following injection of sulfur. (B) at 120°C, left to right: original cobalt particles, 45 sec, 5 min, and 25 min following injection of sulfur (C) at 182°C, left: original cobalt particles, right: shells 1 min after injection of sulfur. The original cobalt particles were synthesized by injecting $Co_2(CO)_8$ in DCB into a solution of oleic acid and TOPO in DCB at 182°C. (D) A summary of the temperature dependence of hollow particle evolution.

(Fig. 1B), and 182°C (Fig. 1C) respectively, with a sulfur-to-cobalt ratio of 4:3 used. The reaction at room temperature is relatively slow. After 1 minute, a thin layer of sulfide appears on the surface of the particles. The nanocrystal solution retains strong

ferrofluidic behavior. Small voids can be observed between the cobalt core and sulfide shell, indicating condensation of vacancies at the boundary. Cobalt cores disappear over time and are not easily distinguishable by TEM after stirring at room temperature for 10 minutes. Small voids are dispersed within each nanocrystal such that there is not enough contrast to clearly reveal a porous structure. At this point, the sample shows a very weak ferrofluidic response to a ~1 Tesla magnet. Gradual coalescence of small voids into bigger ones follows disappearance of visible Co cores. It takes ~19 hours for the appearance of distinguishable hollow nanocrystals in TEM images. At this stage, most nanocrystals have voids inside them although it is still hard to resolve whether there is a single hole within each nanocrystal. These voids are not always located at the center of the spheres and possess quite irregular shapes. Complete consumption of Co can be verified by the absence of any ferrofluidic response of the solution to a magnet. The reaction rate increases dramatically with increase of temperature. At 120˚C, it takes only 45 seconds before an obvious empty gap develops between the core and shell (Fig. 1B). The cobalt core and sulfide shell are seen to be connected by filament-like bridges, resembling structures we previously observed during growth of a selenide shell on Co nanocrystals. These bridges may act as fast transport paths for the delivery of remaining Co onto the shell. The cobalt core disappears quickly, and within 5 minutes a single void with some remaining filaments in the center of the crystals is observed. These remains disappear as the reaction proceeds to completion, leading to hollow nanocrystals with distinguishable, regular, well-centered circular voids in most particles within 25 minutes. The reaction at 182°C usually finishes within seconds, yielding a single circular void located in the center of each particle (Fig. 1C). No intermediate state can be arrested by

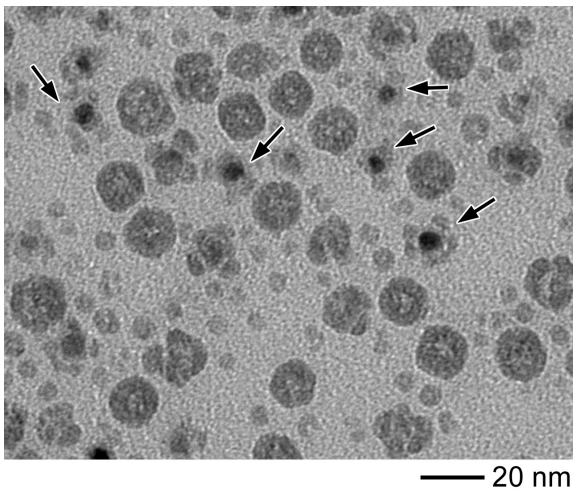

Figure 2. TEM image of the product after reacting cobalt nanocrystals with a sulfur solution at 100°C for 3 minutes. Fracture of some sulfide shells leads to the formation of smaller nanocrystals. Arrows point to the particles at different stages of shell fracture.

manually collecting aliquots at this temperature due to the extremely fast reaction and diffusion rate.

The appearance of multiple voids within each particle upon lowering of the synthesis temperature to room temperature can be attributed to a decrease in vacancy mobilities. Thus, the core and the shell tend not to get separated by a clear gap as seen at higher temperatures. Instead, the shell grows inward incorporating many small voids. These voids coalesce given sufficient time, but since the cobalt core has been consumed before significant coalescence takes place, the tendency for the largest void to form at the center of the particle is visibly reduced. At intermediate temperatures, particles grow according to either mode, with the added complication that TEM images of particles obtained at intermediate reaction stages for reaction temperatures 70-100°C display some shells that look to be either partially fractured or on the verge of fracture (Fig. 2). Although there probably is not significant atom exchange between sulfide shells during

synthesis, even at higher synthesis temperatures, small solid particles with diameter of a few nanometers are often present to a small extent in the product alongside hollow nanocrystals; these may be fragments originating from fracture of growing shells. Thus, we believe that fracture processes occur, albeit less frequently, at higher temperatures as well, but we do not have a theory as to why intermediate temperatures should be most favorable for fracture.

XRD analysis of the reaction at 120°C indicates that the Co_9S_8 phase is kinetically favored although Co_3S_4 is the thermodynamically stable phase at the reaction conditions. Fig. 3 shows XRD patterns of aliquots taken out from a reaction with sulfur-to-cobalt ratio of 4:3 at 120°C (same sample as shown in Fig. 1B) The aliquots were taken out from the hot synthesis solution with a syringe and rapidly injected into an equal volume of anhydrous methanol solution stored under argon at room temperature. After 45 seconds, only Co_9S_8 can be clearly observed by XRD since the remaining Co core is now so small and/or amorphized that its diffraction peaks greatly broaden (Fig. 3a). As the reaction proceeds, Co_9S_8 remains the major phase until the Co core is completely consumed at 25 minutes (Fig. 3b,c). Co_3S_4 has become the dominant phase by 125 minutes, and the change is evidenced by progressive shifting of the major peak position in the patterns as the highest intensity peaks for the two phases overlap, but are ideally offset by ~4° (Fig. 3d). The product collected after 19 hours has been completely converted into Co_3S_4 (Fig. 3e). These results indicate that the formation of Co_3S_4 hollow nanocrystals goes through two separate steps. The first step is the hollowing of cobalt nanocrystals by the outward diffusion of cobalt atoms to form Co_9S_8. The second step is the further transformation of Co_9S_8 to Co_3S_4 while retaining the hollow morphology.

When the same reaction occurs at higher temperatures, the two-step nature of the transformation might be preserved but the intermediate Co_9S_8 particles would be difficult to observe due to the greatly increased reaction and diffusion rate.

As we reported previously, the crystal phase of the product synthesized at high temperature is determined precisely by the molar ratio of cobalt and sulfur in the system. When the sulfur-to-cobalt ratio is less than 8:9 and the reaction is performed at 182°C, XRD analysis reveals the coexistence of Co_9S_8 and metallic Co in the final product.

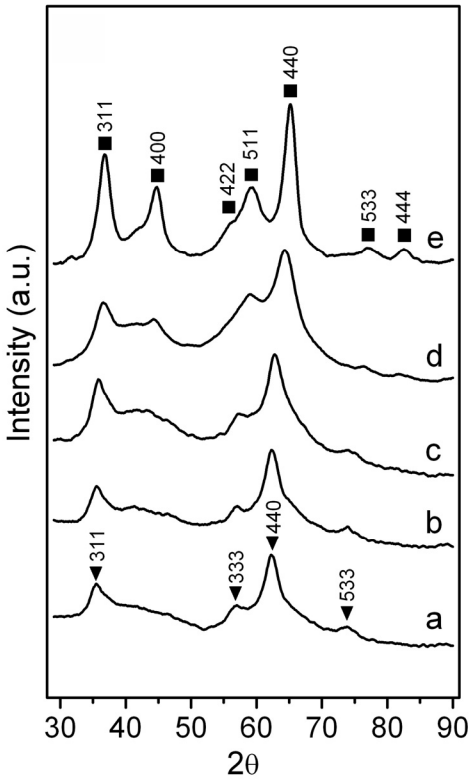

Figure 3. (A) XRD patterns of the sample obtained from the solution after sulfidizing Co nanocrystals at 120˚C for (a) 45 sec; (b) 5 min; (c) 25 min; (d) 125 min; (e) 19 hrs.

TEM inspections show the product to be a mixture of sulfide hollow spheres and solid Co particles. We conclude that the reaction at this temperature finishes before the sulfur

solution can uniformly mix with the Co nanocrystal solution. When the reaction occurs with insufficient sulfur at a lower temperature (e.g. 120°C), the product is a uniform solution of core-shell particles as the reaction rate has been reduced below the time for compete mixing of the sulfur solution into the nanoparticle solution. When the sulfur-to-cobalt ratio is between 8:9 and 4:3, the product is a uniform solution of hollow spheres although XRD pattern shows that it is a mixture of both Co_9S_8 and Co_3S_4 phases. When the sulfur-to-cobalt ratio is greater than 4:3, the product is composed of single phase

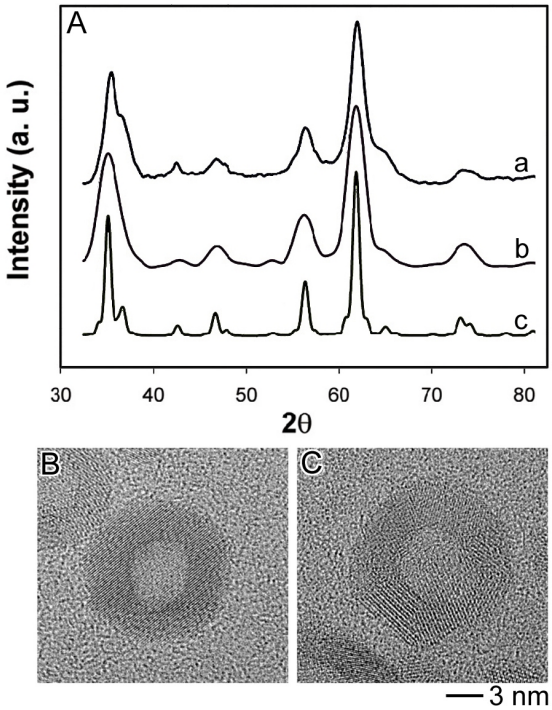

Figure 4. (A) XRD pattern of Co_9S_8 synthesized at 182˚C compared with simulations that illustrate the effect of particle size on peak broadening: (a) the experimental data, (b) the theoretical pattern for a small cubic domain and (c) the pattern expected for a single crystalline hollow shell with dimensions corresponding to TEM measurements of the samples. Experimental peak widths are clearly more consistent with those expected for small domains, implying multi-crystalline shells. A lattice constant of 9.85 Å was used for simulations; the edge length of the cubic domain used in the simulations is 4.2 nm. (B, C) HRTEM images of Co_9S_8 hollow nanocrystals with a single crystalline shell (B) and a multi-crystalline shell (C). The greatly broadened XRD peaks confirm the HRTEM observation of the existence of majority of multi-crystalline shells.

Co_3S_4 hollow nanocrystals.

Kinematical diffraction simulations of the XRD pattern of cobalt sulfide hollow spheres demonstrate that observed peak widths are not consistent with a single crystalline hollow shell of average dimensions seen in TEM images (Fig. 4). Instead, a satisfactory fit to experimental XRD peak widths is obtained by assuming ~4 nm cubic crystalline domains. It can be concluded that each shell is composed of multiple small crystallites. High resolution transmission electron microscopy (HRTEM) confirms that the great majority of sulfide hollow nanocrystals are multi-crystalline (Fig. 4C) although apparently single-crystalline shells are also occasionally observed (Fig. 4B). Typical domain sizes seen in HRTEM images are highly consistent with our interpretation of the XRD patterns. Close inspection of the HRTEM images shows that each crystalline domain extends from the outside surface to inside of the shell, with a neighboring crystal domain present on each side across a grain boundary. The arrangement of the domains is suggestive of the columnar morphology of grains often observed in thin film growth.[19, 20] Co_3S_4 hollow nanocrystals also display the same multi-crystalline structure. If defects such as grain boundaries and cracks formed during shell growth are indeed predominantly aligned along the radial direction, this would tend to provide fast diffusion paths between the inside and outside of the shell. Consistent with this expectation, our previous observation of catalytic activity of Pt nanocrystals encapsulated in hollow CoO nanoshells (prepared by the same methodology as for the sulfide shells) implies that small molecules can penetrate the shells.[1]

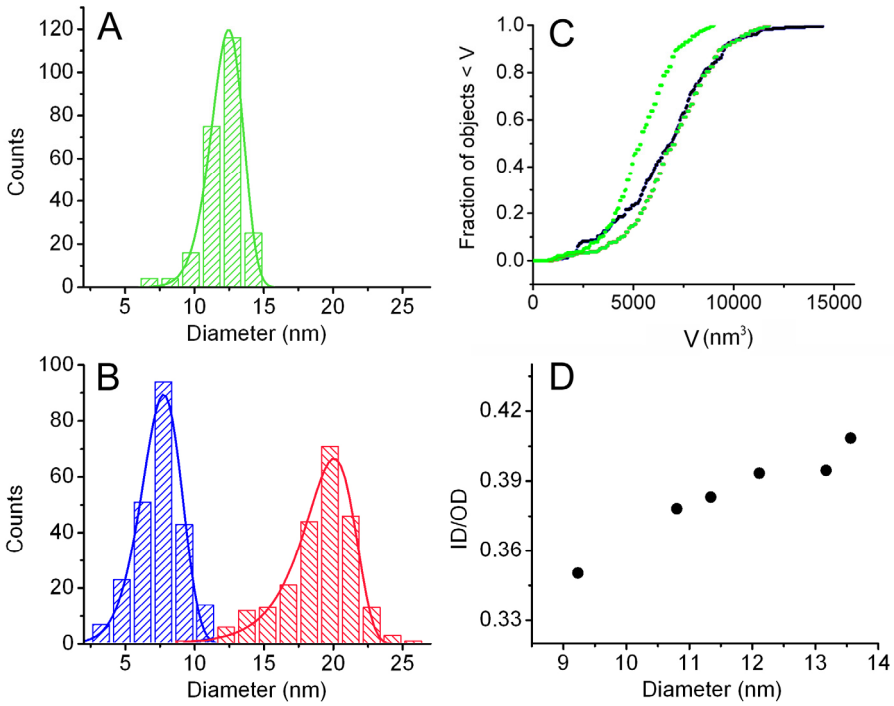

Figure 5. (A, B) Statistics on the sizes of the Co nanocrystals and Co_3S_4 particles in a typical synthesis at 182°C: (A) Histogram of diameters of the original Co nanocrystals; (B) Histogram of inner diameters (left) and outer diameters (right) of the final Co_3S_4 hollow particles. (C) Relationship between the ID/OD ratio of the sulfide shells and the original Co particle size.

If sulfur transport is negligible in comparison to cobalt transport through sulfide shells of nanometer-scale thickness, as has been conclusively demonstrated for growth of much thicker sulfide films on bulk cobalt,[18] final void sizes will closely match the sizes of starting Co nanocrystals. Statistics on the diameters of the original Co and the corresponding Co_3S_4 hollow nanocrystals were taken by measuring the TEM images of a typical sample sulfidized at 182˚C. As shown in Figures 5A and B, the inner and outer diameters of the hollow nanocrystals lie on both sides of the diameters of the original Co nanocrystals. The smaller value of the inner diameter indicates significant inward diffusion of sulfur atoms or inward deformation of the shell during growth. The dispersion of the void sizes (21%) is seen to be roughly twice the dispersion for the initial cobalt particle population (11%), which is consistent with our earlier observations.[1] The

cumulative volume distributions for the initial Co particles and final sulfide shells may be obtained from the same dataset. The initial volume distribution must be scaled by a factor of ~3.8 to match the shell volume distribution on the high end half of the distribution. This value is significantly larger than 3.06, the value based on the molar volume increase upon reaction, implying that 15% of the observed shell volume is porous. The low end of the shell volume distribution is more consistent with little to no porosity; however, determination of void diameter becomes more difficult for smaller particles, so it is difficult to state with certainty that thin shells tend to be more compact.

Statistics on the size of hollow nanocrystals synthesized from cobalt particles at 182˚C with sizes ranging from ~9 nm to ~14 nm were collected to check for dependence of final product morphology on the size of starting materials. Relative void size is expressed as the average ratio between ID and OD providing a measure of the efficiency of the void formation process. The data is displayed in Fig. 5C. The samples show mean ID/OD ratios in the range 30%-45%, smaller than 63%, the value corresponding to the idealized case of immobile sulfur atoms and a stationary Co-Co_3S_4 interface, giving another indication of inward growth or deformation of the shell during shell formation. The increase of the average value of ID/OD with average diameter of original Co nanocrystals in the range of our data suggests that inward growth of the shell mainly occurs at the early stages of growth when a shell is relatively thin.

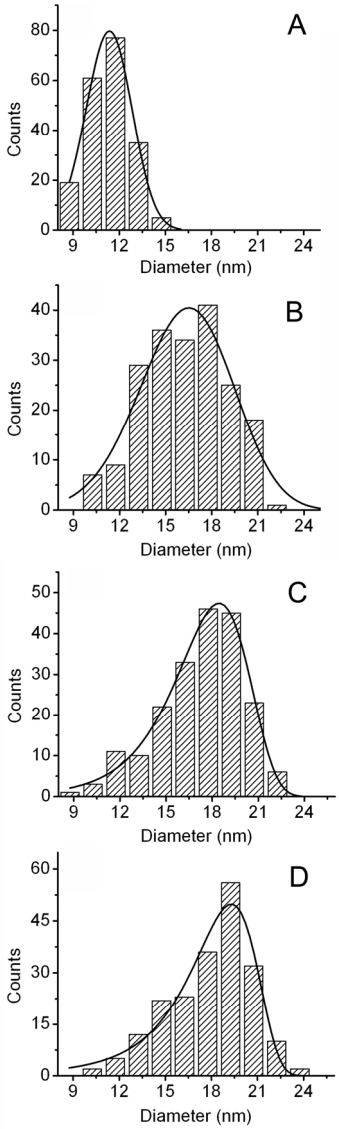

Figure 6. Statistics on the diameter of starting Co nanocrystals (A) and the outer diameter of the sulfide sample obtained after (B) 45 sec; (C) 5 min; (D) 25 min. The Co/S molar ratio is ¾.

Statistics on the sample produced at 120˚C shows the change of size for the population of particles as the sulfidation reaction proceeds: the distribution of outer diameters progressively becomes skewed towards smaller diameters (Fig. 6). This change in shape distributions precedes the appearance of a significant fraction of Co_3S_4 in the diffraction pattern. We did not collect data on the ID distribution at these conditions

and thus cannot compare volume distributions; still, the change of shape remains visible upon comparing distributions of the cube of OD at different times. Fracture of thicker shells as a consequence of stress build-up during growth would remove shells from the high end of the outer diameter distribution and explain the observation. Since further lowering of temperature to 100˚C leads to partially fractured particles in TEM images (Fig. 2) it is reasonable to conclude that the tendency of shells to fracture becomes progressively stronger as temperature is lowered in the temperature range 70-180˚C.

A similar phase change was induced when Co_9S_8 nanocrystals in solution were oxidized by refluxing at 182°C with an O_2/Ar mixture bubbling through. The crystallinity of the nanocrystals decreases dramatically at the onset of the phase transformation. After 5 minutes of exposure to O_2, Co_9S_8 peaks have largely disappeared with only the major (440) peak observable (Fig. 7). At the same time, the (440) peak of Co_3S_4 starts to appear. The peak intensity of Co_3S_4 continues to increase while the Co_9S_8 keeps decreasing. After ~75 min, no Co_9S_8 can be detected. Further heating of the sample with O_2/Ar flow simply improves the crystallinity of the Co_3S_4 nanocrystals and leads to the appearance of two small peaks of CoO, suggesting that the following chemical reaction occurred:

$$2Co_9S_{8\,(s)} + 3O_{2\,(g)} \rightarrow 4Co_3S_{4\,(s)} + 6CoO_{(s)}$$

Assuming that a Co_9S_8 shell transforms into a Co_3S_4 shell with a conformal coating of CoO layer, oxidation of a 4.5-nm thick Co_9S_8 shell is expected to yield a ~4 nm thick Co_3S_4 shell with a ~1 nm CoO coating. If the domain size is equal to the shell

thickness for each compound, we should not be able to observe distinct oxide peaks due to extensive size-broadening. This conclusion is consistent with the fact that no oxide can be detected upon completion of the phase transformation at 75 min. The detection of CoO peaks after prolonged heating indicates significant increase of CoO domain size upon annealing. The intensities of CoO diffraction peaks are weak in comparison to those of Co_3S_4 which is consistent with the smaller volume of CoO formed and its relatively low X-ray scattering power. The hollow nanocrystals before and after oxidation were investigated by using TEM, as shown in Fig. 7B-E. No significant size change was observed, although closer inspection suggests that shells tend to contain

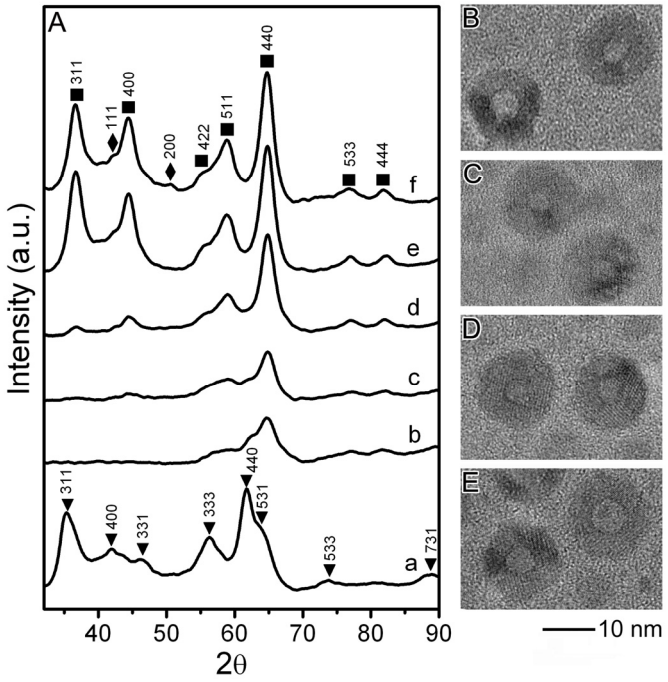

Figure 7. (A) XRD patterns of the sample obtained by heating a Co_9S_8 hollow nanocrystal solution at 182°C with a stream of O_2/Ar (1:4 in volume ratio, 120 ml/min) mixture blowing through for (a) 0 min; (b) 5 min; (c) 15 min; (d) 75 min; (e) 135 min; and (f) 315 min. Co_9S_8 particles were pre-synthesized using a standard procedure with a Co/S ratio of 9/8. (B-E) TEM images of the particles in (a), (c), (d) and (f), respectively.

fewer grains in the final sample. Given the XRD results, the increased crystallinity is likely due to annealing at high temperature.

We also attempted to perform a chemical reduction of the Co_9S_8 hollow nanocrystal dispersion by refluxing at 182˚C with an H_2/Ar mixture flowing through. No phase and size change were observed after the sample was heated for 3 hours. Observed sharpening of XRD peaks with time is readily explained by annealing of the particle at high temperature, lowering average defect density and/or number of grains comprising the shells.

Using non-spherical starting particles can, in principle, yield non-uniform shell thickness due to enhanced reactivity and diffusivity at corners and edges of the particle-shell interface, but we did not observe such an effect using disk-shaped cobalt particles as starting materials. The disks were synthesized using linear amines believed to selectively adhere to basal planes of *hcp*-Co during particle growth to modify final particle morphology. Ferromagnetic interactions among Co disks lead them to pack face-to-face, forming long stacks that lie with the side of the disks in contact with the TEM substrate (Fig. 8A). As shown in Fig. 8B, at first glance most of the particles obtained through sulfidation of Co disks appear to be spherical hollow particles. However, more careful examination of the picture shows some hollow disk shaped boxes viewed edge on. The void diameter and shell thickness for the apparently spherical particles are similar to values measured for disk-shaped particles. This leads us to conclude that all hollow particles in the image are hollow disks, with some happening to lie flat on the substrate. The reduced propensity of disks to stack and stand on their side following sulfidation is explained by the absence of ferromagnetic attraction between them.

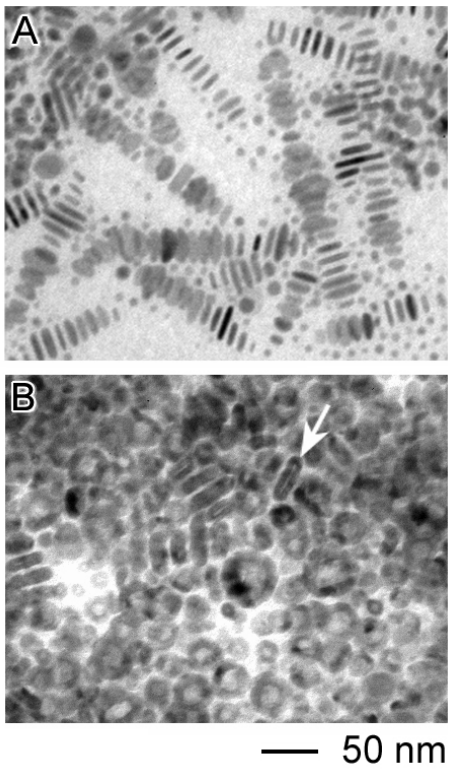

Figure 8. TEM images of (A) disk shaped Co nanocrystals and (B) the product after reacting Co disks with a sulfur solution at 182°C for 3 min. The Co/S ratio is 9:8.

3. Discussion

In the case of a small spherical object, made of a fast-diffusing core material and an outer layer or reservoir of slower diffusing materials, net outward transport of matter from the core and formation of voids are the expected. If the temperature is high enough for vacancies injected into the core region to sample a fraction of the core volume, a significant fraction of the vacancies should end up coalescing into a single large void. Aldinger realized this process experimentally at the micron-scale by annealing a compact of Ni-coated Be powder,[21] and this work is the only example of intentional production of porous materials using the Kirkendall Effect that we know of prior to our work. The

reliance on micron-scale particles and on interdiffusion rather than a highly spontaneous chemical reaction in Aldinger's work necessitated longer reaction times (~5 hrs) and higher temperatures (900˚C) than we employed. The final structures observed by SEM are also more heterogeneous and complex than the relatively uniform structures we obtain for sulfidation temperatures ≥ 120˚C. The less uniform microstructures are likely related to the larger length scales of the starting particles and the final aggregated product being able to support the evolution of a more varied and complex defect structure.

The TEM evidence provided here for significant slowing of void coalescence such that formation of visible voids *lags far behind* complete consumption of Co cores is consistent with porosity due to Kirkendall Effect in confined nanoscale geometries. Other mechanisms proposed to account for emergence of hollow or ring-like structures (e.g. upon oxidation of metal islands on supports) cannot explain the evolution of void morphology with time as a function of temperature in a natural way.

Despite the overall dominance of outward Co transport that leads to void formation, particle statistics demonstrate that significant inward growth and/or deformation of the sulfide shells also occurs through growth. Specifically, it is the magnitude of the void size, characterized either in relation to the average starting particle or as an average of ID/OD for the final product, that demonstrates that the inner boundary of the shell has retreated 1-2 nm from the original cobalt-solution interface. The observed decrease of ID/OD upon increasing starting Co particle size strongly suggests that the inward growth occurs mostly during the early stages of the growth process. The uniformity of the shell thickness as well as near-elimination of the void along the axial direction upon sulfidation of Co disks suggests that both anion and cation mobilities are

high during the formation of the first ~2 nm of sulfide shells, strongly recalling the presence of a reaction zone suggested for cation-exchange reactions performed on nanocrystals.[22] Other justifications may also be involved in the observed inward relaxation; for example, as the synthesis proceeds, initially porous paths allowing for sulfur transport could become sealed or annealed out. In fact, an explanation involving moderate annealing at the synthesis temperature would also explain why an apparent 15% porosity can be seen in thicker shells obtained at 182°C despite the apparent absence of any porosity for thinner shells. Alternatively, compressive stresses created during the growth process may be sufficient to deform the sulfide shells when they are thinner. It is quite likely that a combination of processes determine the extent of inward growth.

Another deviation from behavior extrapolated from bulk studies involves the transformation of Co to Co_3S_4. In bulk sulfidation, the sulfide films support multiple phases, with a progression from cobalt-rich to sulfur-rich phases as one moves outwards from the cobalt-vapor interface. In contrast, X-ray diffraction characterization suggests a two-step transformation where the final product, Co_3S_4 does not appear until all cobalt has disappeared. Since diffraction would not be sensitive to amorphous or very highly defected domains of Co or Co_3S_4, this finding may merit, in the future, verification with a chemically sensitive technique. However, at least in the case of Co_3S_4, one can argue that it is likely to nucleate in relatively defect-free domains: The transformation of a Co_9S_8 shell into a Co_3S_4 shell may be facilitated by the identical arrangement of sulfur anions in the two structures except for a slightly larger separation of the anions in Co_3S_4.

We have provided a number of observations which, when taken together, raise the possibility of propensity of shells to fracture within a range of the synthesis temperature.

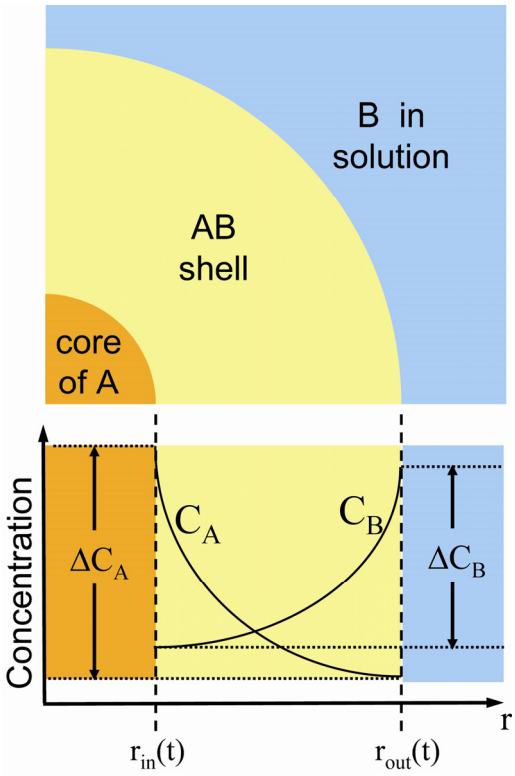

Figure 9. Explanation of terms used in the derivation in the text. The positions of the shell-solvent and shell-core interfaces are measured radially and are a function of time.

Small solid fragments of cobalt sulfide are present, to some extent, at all synthesis temperatures we have studied; however, apparently disintegrating shells in TEM images (for synthesis at 100°C) and statistically significant changes in the skewness of the shell volume distribution are only seen at a lower (120°C) temperature. A natural explanation is that fracture occurs, to some degree, over the complete temperature range that we have studied, but that higher temperatures result in relaxation of growth stresses and improve the adhesion between the core and the shell. The particles obtained at room temperature do not follow this proposed trend: no signs of fracture are seen in TEM images. However, given the very different mode of growth observed at this temperature, this may not necessarily contradict our interpretation. The calculated ratio of the volume of sulfide

produced to the volume of cobalt consumed in the reaction is 2.4 for formation of Co_9S_8 and 3.1 for Co_3S_4. For oxidation of metals, this ratio is referred to as the Pilling-Bedworth ratio and is used as an empirical predictor of whether the metal oxide layer that forms on a metal surface will be a protective (passivating) or not. Most oxides with a value of Pilling-Bedworth ratio > 2 develop large stresses during growth, leading to cracking, buckling or spalling. Presumably, the absence of such processes in bulk sulfidation experiments is due to relaxation of growth stresses at the higher temperatures (~900°C) used. The relatively large volume change upon sulfidation supports our interpretation of fracture during shell growth.

Continuum models of the diffusional processes can provide a semi-quantitative picture of asymmetric net matter flows during growth of a shell of compound A_mB_n around a core of pure material A suspended in a reservoir of pure material B. A sophisticated model based on time-dependent diffusion kinetics and interfacial motion relating to interdiffusion in a spherical diffusion couple has been presented in the literature.[23] While such models should provide numerically accurate descriptions of the early stages of growth, void coalescence and its impact upon subsequent evolution of the hollow morphology cannot be addressed without introducing additional processes and parameters.

Here, we proceed by making a large number of simplifying assumptions. Most notably, we assume that the *time-independent* diffusion equation applies, that electric field driven enhancement of ion transport well-known in growth of very thin (1 nm) oxide films can be neglected, that the shell is of uniform thickness, that the core material can access the shell with equal ease throughout the growth process and that interfaces

remain sharp. Furthermore, we assume that the core material is transported outwards with sufficient speed such that inward growth of the shell is not impeded by stress at the interface. It may be difficult to find synthesis conditions where all of these assumptions hold simultaneously, but this picture offers an idealized benchmark to compare experimental results to. Furthermore, some relevant dimensionless parameters should emerge from this very basic treatment.

Fig. 9 summarizes the terms of the derivation. Position is measured radially from the center of mass of the initial nanoparticle whose radius is taken to be unity. The position of the inner boundary of the growing A_mB_n shell at time t is denoted $r_{in}(t)$ and the position of the outer boundary (the A_mB_n/solution interface) at time t is denoted $r_{out}(t)$. The magnitude of the flux for species i, J_i at radial position r is predicted by the steady-state diffusion equation at time t and has the simple form,

$$\left|J_i\right| = \frac{D_i \Delta C_i}{r^2} \times \frac{r_{in}(t) r_{out}(t)}{r_{out}(t) - r_{in}(t)},$$

where D_i refers to the diffusion coefficient for the transport of either species A or species B through the AB phase and ΔC_i refers to the concentration drop for that species across the AB shell. It is reasonable to treat ΔC_i as constants whose values are maintained throughout shell growth by contact of the shell with pure A on the internal surface and excess dissolved B on the outer surface. The inward growth rate of the shell should be proportional to the inward flux of B at $r = r_{in}(t)$ and outward growth of the shell should be proportional to the outward flux of A at $r = r_{out}(t)$. Assuming that the previous equation holds, this leads to the ratio of the inward and outward growth rate satisfying

$$\left| \frac{dr_{out}}{dt} \middle/ \frac{dr_{in}}{dt} \right| = -\frac{n \cdot D_A \left|\Delta C_A\right|}{m \cdot D_B \left|\Delta C_B\right|} \times \left[\frac{r_{in}(t)}{r_{out}(t)} \right]^2 .$$

The time infinitesimals on the left side may be cancelled, yielding a differential equation relating r_{out} and r_{in}. When the initial condition $r_{in}(t_0) = r_{out}(t_0) = 1$ is imposed on this equation, it yields an algebraic relationship between r_{in} and r_{out} that holds throughout shell growth,

$$r_{out}(t)^3 + K \cdot r_{in}(t)^3 = 1 + K , \qquad (1)$$

with $K = \dfrac{n \cdot D_A |\Delta C_A|}{m \cdot D_B |\Delta C_B|}$.

The reaction is completed when the volume of the shell matches the value expected from the initial particle volume, i.e. when $r_{out}(t)^3 - r_{in}(t)^3 = V_{AB}$, where V_{AB} is the volume of compound AB produced per volume of initial starting material A. Fig. 10 illustrates the time evolution of $r_{in}(t)$ and $r_{out}(t)$ and the application of the volume balance for different values of V_{AB} to determine the time for completion of the reaction and the final geometry. Combining this 'volume balance' with expression (1), we obtain for the final product geometry,

$$\frac{ID}{OD} = \left[\frac{1 + K - V_{AB}}{1 + K + KV_{AB}} \right]^{1/3} \qquad (2)$$

where we have used ID/OD instead of r_{in}/r_{out} since it emphasizes that ID/OD is a reasonable measure of the extent of outward growth of the shell within an idealized model.

An interesting feature of expression (2) for ID/OD is that it predicts negative void diameters for $K < (V_{AB} - 1)$. In Fig. 10, this situation corresponds to the shell volume still being smaller than V_{AB} at the time that ID reaches zero. In this regime, the assumption of unopposed inward growth of the shell becomes unphysical as a finite amount of the

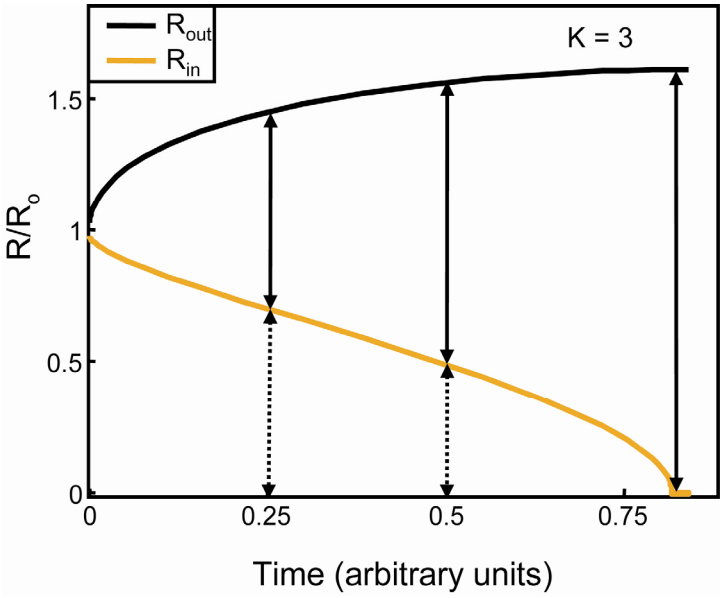

Figure 10. Numerically determined solution of the model explained within text corresponding to a value of 3.0 for the parameter, K. A particular shell volume is expected to be obtained for a particular choice of the materials A, B and AB. The volume increase upon reaction is used to determine the time for completion and determines the final void size (dashed arrows) and shell thickness (solid arrows).

relatively immobile core material is assumed within the model to be confined into a region of zero diameter. Thus,

$$\frac{n \cdot D_A |\Delta C_A|}{m \cdot D_B |\Delta C_B|} > (V_{AB} - 1) \qquad (3)$$

is a minimum condition for the production of hollow structures. When this condition is violated, the rate of inward growth of the shell becomes limited by the rate of removal of core material, i.e. by the outward growth rate and the structures obtained are likely to be solid shells with core-shell structures observed at intermediate stages of growth. Within this idealized picture, regardless of whether the final structure is hollow or solid, the order of magnitude of the reaction time is dictated by the diffusivity of the core species through the compound shell and not by the diffusivity of the dissolved species.

At elevated temperatures, voids in hollow particles are expected to decrease in size with time due to the Gibbs-Thomson Effect. The time required for the elimination of a central void in a hollow was estimated recently to be:[24]

$$t_{shrink} \approx \frac{l^3 kT}{10\gamma D\Omega}$$

with γ and Ω denoting the surface energy of the shell material and the volume of a vacancy respectively and l corresponding to initial size of the void. One condition for controllable synthesis is that t_{shrink} be much smaller than the typical timescale of a synthesis. For the case of a purely immobile dissolved species (i.e. K = 0) and for reasonable values of $V_{AB,}$ the time for hollow shell formation to complete within our model is approximately

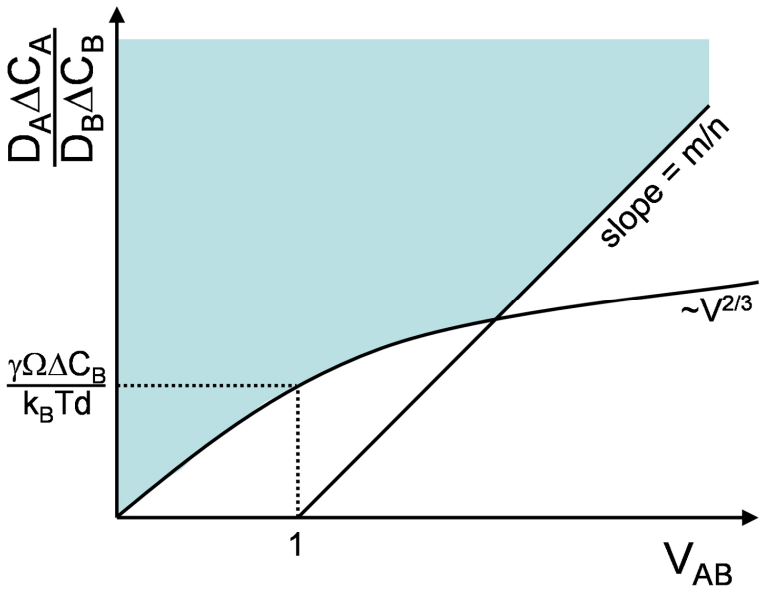

Figure 11. Diagram summarizing the two different criteria for hollow particle formation that relate the diffusivities and concentration drops across the shell for the species A and B with the volume change upon reaction. The shaded area corresponds to the region where hollow particle formation is allowed. The variables shown are defined in the text.

$$t_{synth} \approx \frac{d^2 V_{AB}^{2/3}}{6 D_A \Delta C_A}.$$

In this expression, concentration C_A refers to the (dimensionless) local volume fraction of A in the compound AB. The time for void closure is seen to increase more strongly with particle size in comparison to the time required for the shell formation. Presumably, this arises from the fact that the driving force for the void closure process is the size dependent Gibbs pressure, whereas we assumed a size-independent free energy of reaction to be driving the hollow shell formation. Noting that in a hollow shell of compound AB, it is the diffusivity of the slower species, assumed here to be species B, that limits inward relaxation of the shell, we can write,

$$\frac{t_{shrink}}{t_{synth}} = \frac{3}{5} \times \frac{\Delta C_A}{V_{AB}^{2/3}} \times \frac{kT_{synth} d}{\gamma \Omega} \times \frac{D_A}{D_B} \qquad (4)$$

where each fraction on the right hand side is dimensionless. For hollow particles to be stable at the synthesis temperature, $t_{shrink} >> t_{synth}$. Using reasonable orders of magnitude for synthesis of Co_3S_4 particles, $\gamma \sim 1000$ mJ/m^2, $T_{synth} = 450$ K, $\Omega \sim (1\ Å)^3$, d = 9 nm, $\Delta C_A \sim 0.01$, $V_{AB} = 3.06$, the condition becomes, roughly, $D_A/D_B > 10$. In contrast, assuming $\Delta C_{Co} \sim \Delta C_S$, Eqn. 3 requires $D_A/D_B > 2.7$. In other words, requiring voids to be stable during the minimum timescale for synthesis sets the more stringent requirement on relative diffusivities of Co and S atoms in our system. Diffusivity of sulfur is seen to be negligible during growth of sulfide films on bulk cobalt and suggesting that $D_{Co}/D_S >> 10$. Thus, growth by a diffusive mechanism is a feasible explanation of the observation of voids in our system.

The requirements stated in Eqn.s 3 and 4 may be summarized by the schematic 'phase diagram' shown in Fig. 11. Both axes of the diagram are dimensionless

parameters: the vertical axis is the ratio $D_A\Delta C_A/D_B\Delta C_B$ and the horizontal axis is V_{AB}. The inequality in Eqn. 3 is represented in this plot by the region above a line of slope of m/n (roughly unity) passing through $V_{AB} = 1$. Eqn. 4, on the other hand, corresponds to a region above a curve of form $V^{2/3}$ with its overall height set by the parameter $\gamma\Omega\Delta C_B/kTd$. The region lying above both curves corresponds to the combination of material parameters that allow for synthesis of hollow particles.

4. Conclusion

In summary, we investigated in detail the formation of cobalt sulfide hollow nanocrystals through a Kirkendall-like mechanism in nanometer scale materials. Performing the reaction at 'high' (>120˚C) temperature leads to fast formation of a single void inside each shell while reaction at room temperature leads to the formation of multiple voids, which can be attributed to strongly temperature-dependent diffusivities for vacancies. Although the void formation process is dominated by the outward diffusion of cobalt cations, there is still significant inward transport of sulfur anions as inferred from the fact that the inner diameter of the shell is smaller than the original cobalt nanocrystals. Volume distributions for initial and final nanostructures imply that sulfide shells grown at high temperature contain extra volume comparing to the value calculated by assuming a single crystal material, indicating significant porosity and/or defective structure. At intermediate temperatures (100-120˚C), we observe indirect and direct signs of fracture occurring upon during shell formation. In addition, in this temperature range, formation of the Co_3S_4 phase proceeds slowly enough to enable observation of a two step process: Co is sulfidized into Co_9S_8 which subsequently

transforms into Co_3S_4. The physical mechanism behind inward growth of the shell might involve bulk deformations of the shell or transport of sulfur through cracks in the shell. A highly idealized model provides two different dimensionless combinations of material parameters that indicate whether shell growth is obtainable in principle for a specific choice of starting materials.

Within the cobalt sulfide system, we believe that significant inward growth or deformation of a shell occurs during the early stages of growth. As growth temperature is lowered, the final product becomes more complex: shell fracture may occur and/or multiple voids may be produced within each particle at lower temperatures. Alternative mechanisms may be proposed for many of our observations and further studies, both experimental and theoretical, are needed to arrive at a more conclusive understanding. We believe that the general concept of formation of hollow nanocrystals using the Kirkendall effect can be extended compositionally to the synthesis diverse material classes including metals, semiconductors and insulators. Furthermore, the production of hollow disk shaped boxes that we presented indicates that the procedure reproduces the shape of the original nanocrystals in the final porous product. Utilizing starting materials where shape control has been established, forming hollow particles and chemically modifying the product using procedures that preserve particle porosity and morphology, it should be possible to combine a strong degree of shape and compositional control in the production of hollow nanostructures.

5. Experimental

Oleic acid (OA, 99%), anhydrous *o*-dichlorobenzene (DCB, 99%), sulfur (99.998%), and hexadecylamine (HDA, 99%) were purchased from Sigma-Aldrich. Dicobalt octacarbonyl $Co_2(CO)_8$ containing 1-5% hexane as a stabilizer and trioctylphosphine oxide (TOPO, 90%) were purchased from Alfa Aesar. Oleic acid, $Co_2(CO)_8$, and DCB were stored in an argon filled glovebox. TOPO and HDA were stored under air.

The preparation of cobalt sulfide hollow nanocrystals consisted of two steps: synthesis of a Co nanocrystal dispersion and reaction of the nanocrystals with dissolved molecular sulfur. Co nanocrystals were synthesized using an airless procedure reported previously.[25] The synthesis involves fast injection of a solution of $Co_2(CO)_8$ into a hot mixture of organic solvent and surfactants under inert atmosphere. The carbonyl rapidly decomposes, yielding carbon monoxide and dissolved cobalt species. Nucleation of Co nanocrystals occurs within seconds after the injection. A small amount of surfactant molecules is present in the synthesis mixture to prevent agglomeration and coalescence of the forming nanoparticles. The size and size dispersion of the resulting particles may be controlled by the composition of the surfactant mixture used, the surfactant:precursor:solvent ratio, the reaction temperature and the growth time.[26] Using a surfactant mixture composed of OA and TOPO yields uniform spherical ε-Co nanocrystals. The addition of an amine such as HDA to the same synthesis results in the formation of disk-shaped nanocrystals of *hcp*-Co.[27] The cobalt sulfide hollow nanocrystals are prepared by adding molecular sulfur dissolved in DCB into the Co nanocrystal solution.

In a typical synthesis, 0.1 g TOPO is degassed with Ar at 60˚C in a three-neck flask for about 20 min, followed by introduction of a solution of 0.1 mL of OA in 15 mL of DCB prepared under Ar. The mixture is heated to the reflux temperature (~182˚C). A precursor solution of 0.54 g of $Co_2(CO)_8$ in 3 mL of DCB is prepared separately under Ar and rapidly injected into the hot surfactant solution under vigorous stirring. The temperature usually drops to 165-170˚C upon injection of the precursor solution but returns to refluxing within 10-30 seconds. The decomposition of $Co_2(CO)_8$ results in a black ferrofluidic dispersion within a few seconds. A solution of cobalt nanocrystals with uniform size can be collected within 15-60 seconds of the injection. The size distribution subsequently broadens as the nanocrystals start to ripen. Therefore, within a minute of injection of the Co precursor, an air-free solution of 0.128 g of elemental sulfur in 5 mL DCB was injected into the Co nanocrystal dispersion. The solution was heated under stirring for another three minutes, removed immediately from the hot flask into an Ar filled vial and cooled to room temperature. The solution of particles remains stable despite complete sulfidation of particles, suggesting that surfactant molecules also stabilize sulfide nanocrystals by dynamically coating the surfaces of the particles. For synthesis of disk shaped cobalt nanocrystals, 0.61 g of HDA was added to the surfactant solution in addition to TOPO and OA, allowing anisotropic growth of nanocrystals. The sulfidation step proceeded identically to the procedure used for spherical particles. In order to investigate the evolution of the morphology and crystal structure of the nanocrystals, aliquots of the synthetic mixture were collected during reaction and immediately cooled down to room temperature.

Hollow nanocrystals can be cleaned or extracted from the original solution by using the same method reported for cleaning Co nanocrystals. Typically, an equivalent volume of anhydrous alcohol is added to the original solution and centrifuged at ~3000 rpm for 5 min. The supernatant is decanted and the black precipitate can be redissolved with other nonpolar solvents. The binding of surfactants to the sulfide surface seems to be weaker than that to the metallic cobalt surface as the addition of methanol to the solution usually strips the surfactant layer and leads to irreversible aggregation. Alcohols with longer chains such as 2-propanol are less aggressive and improve the re-dispersibility of the precipitate.

The crystal structure of the samples was measured using powder X-ray diffraction with Co Kα radiation (1.790 Å) and a general area detector (GADDS, Bruker). The instrument resolution is 0.05° in 2θ, and the accumulation time for each sample was 20 min. XRD samples were prepared by depositing a precipitated powder on a quartz plate. Nanocrystal size, morphology, structure, and superstructures were probed by Transmission Electron Microscopy (TEM) at the National Center for Electron Microscopy at the Lawrence Berkeley National Laboratory, on a JEOL CX200 and a Tecnai G^2 S-Twin electron microscope (200 kV). TEM samples were prepared by placing a drop of the nanocrystal solution onto a carbon-coated copper grid at room temperature.

Acknowledgement:

This work was supported by the Air Force Office of Scientific Research under award no. FA9550-04-1-0065 and by the Director, Office of Energy Research, Office of Science,

Division of Materials Sciences, of the U.S. Department of Energy under contract no. DE-AC02-05CH11231. AC thanks financial support from the Generalitat de Catalunya, Departament d'Universitats, Recerca i Societat de l'Informacio.

[1] Y. Yin, R. M. Rioux, C. K. Erdonmez, S. Hughes, G. A. Somorjai, A. P. Alivisatos, *Science* **2004**, *304*, 711.

[2] H. J. Fan, R. Scholz, F. M. Kolb, M. Zacharias, U. Gösele, *Solid State Comm.* **2004**, *130*, 517.

[3] Y. Sun, Y. Xia, *Science* **2002**, *298*, 2176.

[4] Y. Sun, B. T. Mayers, Y. Xia, *Nano Lett.* **2002**, *2*, 481.

[5] L. Guo, C. J. Murphy, *Nano Lett.* **2003**, *3*, 231.

[6] D. Farrell, S. A. Majetich, J. P. Wilcoxon, *J. Phys. Chem. B* **2003**, *107*, 11022.

[7] E. O. Kirkendall, *Trans. AIME* **1942**, *147*, 104.

[8] A. D. Smigelskas, E. O. Kirkendall, *Trans. AIME* **1947**, *171*, 130.

[9] G. B. Gibbs, *Oxid. Met.* **1973**, *7*, 173.

[10] Y. Chang, J. J. Teo, H. C. Zeng, *Langmuir* **2005**, *21*, 1074.

[11] B. Liu, H. C. Zeng, *J. Am. Chem. Soc.* **2004**, *126*, 16744.

[12] C. M. Wang, D. R. Baer, L. E. Thomas, J. E. Amonette, J. Anthony, Y. Qiang, G. Duscher, *J. Appl. Phys.* **2005**, *98*, 094308.

[13] E. G. Derouane, J. J. Chludzinski, R. T. K. Baker, *J. Cat.* **1984**, *85*, 187.

[14] T. Wang, L. D. Schmidt, *J. Cat.* **1981**, *71*, 411.

[15] T. Nakayama, M. Arai, Y. Nishiyama, *J. Cat.* **1983**, *79*, 497.

[16] J. J. Chen, E. Ruckenstein, *J. Phys. Chem.* **1981**, *85*, 1606.

[17] J. Tang, M. Myers, K. A. Bosnick, L. E. Brus, *J. Phys. Chem. B* **2003**, *107*, 7501.

[18] S. Mrowec, M. Danielewski, A. Wojtowicz, *J. Mater. Sci.* **1998**, *33*, 2617.

[19] B. A. Movchan, A. V. Demchishin, *Fiz. Met. Metalloved.* **1969**, *28*, 653.

[20] J. A. Thornton, *J. Vac. Sci. Tech.* **1974**, *11*, 666.

[21] F. Aldinger, *Acta Metal.* **1974**, *22*, 923.

[22] D. H. Son, S. M. Hughes, Y. Yin, A. P. Alivisatos, *Science* **2004**, *306*, 1009.

[23] R. A. Masumura, B. B. Rath, C. S. Pande, *Acta Mater.* **2002**, *50*, 4535.

[24] K. N. Tu, U. Gösele, *Appl. Phys. Lett.* **2005**, *86*, 093111/1.

[25] V. F. Puntes, K. M. Krishnan, A. P. Alivisatos, *Appl. Phys. Lett.* **2001**, *78*, 2187.

[26] V. F. Puntes, K. M. Krishnan, A. P. Alivisatos, *Science* **2001**, *291*, 2115.

[27] V. F. Puntes, D. Zanchet, C. K. Erdonmez, A. P. Alivisatos, *J. Am. Chem. Soc.* **2002**, *124*, 12874.